Observing Self-Assembled Lipid Nanoparticles Building Order and Complexity through Low-Energy Transformation Processes

Xavier Mulet,[†] Xiaojuan Gong,[‡,§] Lynne J. Waddington,[⊥] and Calum J. Drummond[†,∥,*]

[†]CSIRO Molecular and Health Technologies, Bag 10, Clayton South MDC, VIC 3169, Australia, [‡]CSIRO Molecular and Health Technologies, Riverside Life Sciences Centre, North Ryde, NSW 2113, Australia, [§]School of Chemistry, F11, The University of Sydney, NSW 2006, Australia, [⊥]CSIRO Molecular and Health Technologies, 343 Royal Parade, Parkville, VIC 3052, Australia, and [∥]CSIRO Materials Science and Engineering, Bag 33, Clayton South MDC, VIC 3169, Australia

ABSTRACT Future nanoscale soft matter design will be driven by the biological paradigms of hierarchical self-assembly and long-lived nonequilibrium states. To reproducibly control the low-energy self-assembly of nanomaterials for the future, we must first learn the lessons of biology. Many cellular organelles exhibit highly ordered cubic membrane structures. Determining the mechanistic origins of such lipid organelle complexity has been elusive. We report the first observation of the complete sequence of major transformations in the conversion from a 1D lamellar membrane to 3D inverse bicontinuous cubic nanostructure. Characterization was enabled by adding a steric stabilizer to dispersions of lipid nanoparticles which increased the lifetime of very short-lived nonequilibrium intermediate structures. By using synchrotron small-angle X-ray scattering and cryo-transmission electron microscopy we observed and characterized initial lipid bilayer contacts and stalk formation, followed by membrane pore development, pore evolution into 2D hexagonally packed lattices, and finally creation of 3D bicontinuous cubic structures.

KEYWORDS: lamellar phase · inverse bicontinuous cubic phase · transition · cryo-TEM · synchrotron SAXS

More than 40 years ago, Luzzati *et al.* showed that lipids can self-assemble into a variety of ordered aggregate structures with nanoscale repeat units and a diversity of complexity.[1] Knowledge of lipid polymorphism has markedly increased between then and now, with particular interest being placed on the inverse bicontinuous cubic structures and their applications and role in nature.[2−7] The inverse bicontinuous cubic phases consist of a lipid bilayer draped over a triply periodic minimal surface (TPMS). These include the primitive (the Q_{II}^{P} phase with space group *Im*3*m*), double diamond (Q_{II}^{D} phase with space group *Pn*3*m*), and gyroid (Q_{II}^{G} phase with space group *Ia*3*d*) TPMSs.[8,9]

These nanostructured high surface area self-assembly materials are finding application in a range of end uses including drug delivery,[7] material templating,[10] and membrane protein crystallography.[11,12] Cubic nanostructures are also present in many organelles within different organisms[13] such as the endoplasmic reticulum[14] and mitochondrial inner membranes.[15] The transition from the lamellar phase to the cubic phase is regarded as a structural model of biomembrane lipid scaffold remodeling events such as endocytosis.[16] Such complex 3D membrane reorganization processes have also been observed during skin barrier morphogenesis and a model of intersection-free membrane unfolding has been proposed.[17,18] Advancing the understanding of how lipids build structural order and complexity is a key element in progressing bottom-up nanofabrication processes based on amphiphile self-assembly.

In this article we characterize the transformation from a simple one-dimensional (1D) planar membrane system to a more complex three-dimensional (3D) organelle-like network of nanochannels, where the dimensionality refers to the underlying crystal lattice. In particular we focus on the transition between the fluid lamellar (L_α) lyotropic liquid crystalline phase adopted by eukaryotic cell membranes and the double diamond inverse bicontinuous cubic phase (Q_{II}^{D}). We have been able to control the transition rate between the two mesophases and this has allowed us to observe the intermediates during the formation of the 3D network.

A dynamic, nonequilibrium transition is by its very nature typically difficult to observe—it shows little order, cannot be resolved by standard X-ray diffraction

*Address correspondence to calum.drummond@csiro.au.

Received for review June 24, 2009 and accepted August 11, 2009.

Published online August 31, 2009.
10.1021/nn900671u CCC: $40.75

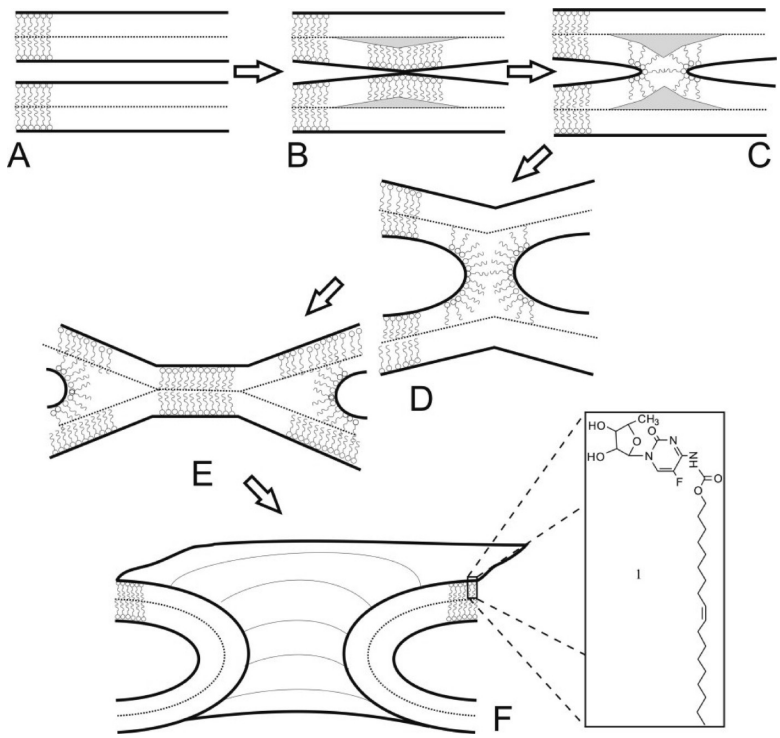

Figure 1. Structure of lipid derivative 1, 5′-deoxy-5-fluoro-*N*4-(cis-9-octadecenyl-oxycarbonyl) cytidine. Model of pore or ILA formation events: (A) initial Lamellar phase; (B) thermal undulations lead to membrane contact (C,D), which then develops into a stalk formation (E) and possibly a transmembrane contact (TMC) also referred to as a hemifusion diaphragm; (F) this state can then form a pore, also known as an interlamellar attachment (ILA).

techniques, and cannot be directly imaged owing to its short lifetime. In the present work, experimental observations were made using cryo-transmission electron microscopy (cryo-TEM) and synchrotron small-angle X-ray scattering (SAXS). The two complementary techniques have allowed us to probe different spatial length scales which correlate strongly. The use of a block copolymer stabilizer has permitted us to link the temporal length scales of the different techniques. We are thus able to propose a comprehensive model of the L_α to Q_{II}^D phase transition which we believe to be generally applicable to transitions between the fluid lamellar phase and inverse bicontinuous cubic phases, and potentially also inverse hexagonal phases.

RESULTS AND DISCUSSION

To date, observation of the nonequilibrium process of phase transitions, beginning with membrane fusion, has been elusive. Nevertheless, a model of the initial events (summarized in Figure 1) has been proposed that to some extent has been confirmed by experiments.[19,20] The most common model of fusogenic processes has inherent specific structures for the intermediates that lead to membrane fusion and pore formation. The stalk model of membrane fusion consists of merged cis-monolayers and noncontacting trans-monolayers (see Figure 1D), which can then form a pore or interlamellar attachment (ILA).[21] The next intermediate that has been proposed may include a transmembrane contact (TMC, see Figure 1E).[22] Following rupture of the hemifusion diaphragm, the formation of the pore is complete (Figure 1F).

The structure of the lipid derivative **1** used in this study is shown in Figure 1. Lipid derivative **1** is a novel amphiphile pro-drug currently being investigated in our group as a chemotherapeutic agent where amphiphile self-assembly provides a means to control the release profile of the bioactive. The chosen lipid derivative is ideal for the present investigation as it exhibits a temperature induced L_α to Q_{II}^D phase transition at 33 °C under excess water conditions. This lipid can be prepared as a nanoparticulate dispersion in water, sterically stabilized with the block copolymer Poloxamer 407 (Supporting Information, Figure S1) to form particles of approximately 200 nm. Sample preparation is outlined in the methods section of this manuscript. To observe lyotropic liquid crystalline phase transformation behavior, the different dispersions were heated at 5 °C min^{-1} from 25 to 70 °C: a temperature jump. Synchrotron SAXS was then used to follow the Bragg reflections of the various phases, including intermediate phases, formed during the transformation and to calculate their lattice parameters (Figure 2).

During a transformation of the system in the absence of Poloxamer, as shown in Figure 2A, the phase sequence is as expected from an increase in temperature—the crystalline lamellar phase is replaced by a fluid lamellar and then a Q_{II}^D phase. Both the L_α and Q_{II}^D phases show a decrease in lattice parameter, previously seen for similar transitions and explained partially with respect to changing hydrocarbon chain isomerism with increased temperature and partially to the effect of water diffusion throughout the sample.[19] The thermally induced transitions yield smooth transformations with no visible intermediates. Any intermediates with short (millisecond) lifetimes would not be captured in such an experiment. It should be noted that the absence of steric stabilizer leads to rapid nanoparticle aggregation.

For those samples containing Poloxamer (Figure 2B−D) we note the presence of an additional intermediate phase, presumably stabilized by Poloxamer, to lower scattering angle (see Supporting Information, Table S1 for lattice parameter summary). This intermediate has a large lattice parameter that decreases with time as the cubic phase begins to form. In conjunction with the cubic phase appearance, the scattered intensity of the intermediate phase is reduced. This intermediate occurs during the fluid lamellar to cubic phase transition and is metastable throughout the lifetime of the L_α phase. It has been suggested that the presence of sterically large molecules will slow down the rate of

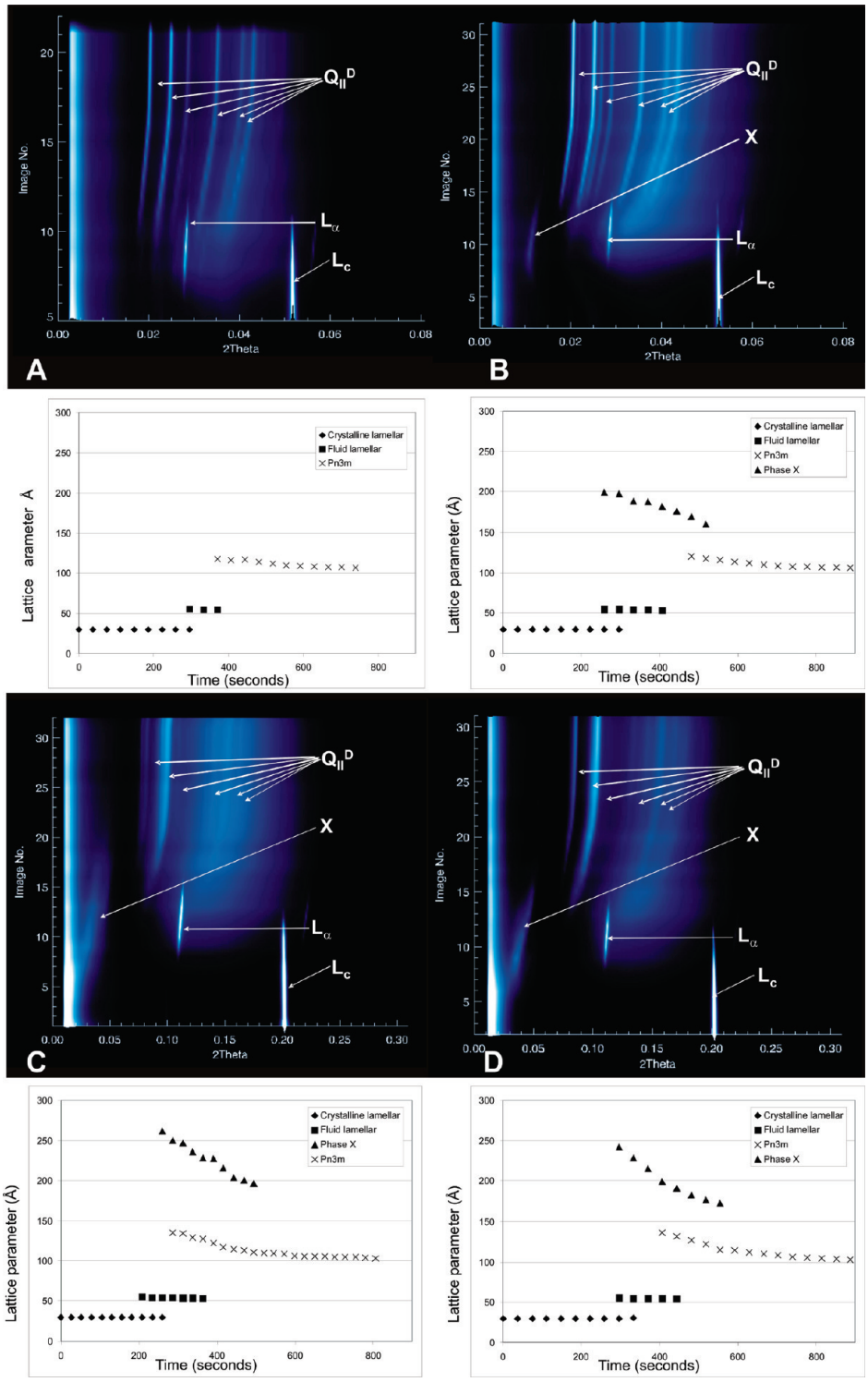

Figure 2. Synchrotron SAXS integrated diffraction patterns showing phase changes for nanoparticles of lipid derivative 1 in water during a temperature jump as a function of time. Lipid 1 makes up 10 wt % of total sample mass. Below each phase sequence are the lattice parameters of the different mesophases observed. In all sequences a transition from the lamellar crystalline (Lc, first Bragg reflection shown), to fluid lamellar (L_α 1, $\sqrt{4}$ Bragg reflections visible) followed by double diamond cubic (Q_{II}^{D}, *Pn3m*, $\sqrt{2}$, $\sqrt{3}$, $\sqrt{4}$, $\sqrt{6}$, $\sqrt{8}$ and $\sqrt{9}$ Bragg reflections visible) can be observed. Panels B through D also show the presence of a broad unresolved intermediate peak at low scattering angles. The different sample compositions are (A) lipid 1 with 0 wt % Poloxamer, (B) lipid 1 with 0.5 wt % (of total sample mass) Poloxamer, (C) lipid 1 with 1 wt % (of total sample mass) Poloxamer, (D) lipid 1 with 1 wt % (of total sample mass) Poloxamer and 5 wt % (of total sample mass) ethanol.

phase transition.[23] This pertinent observation suggests that a structural intermediate has been stabilized by the presence of the triblock copolymer to form a relatively long-living metastable phase. We propose that this highly hydrated structure is the previously reported phase X, considered to be a precursor to the cubic

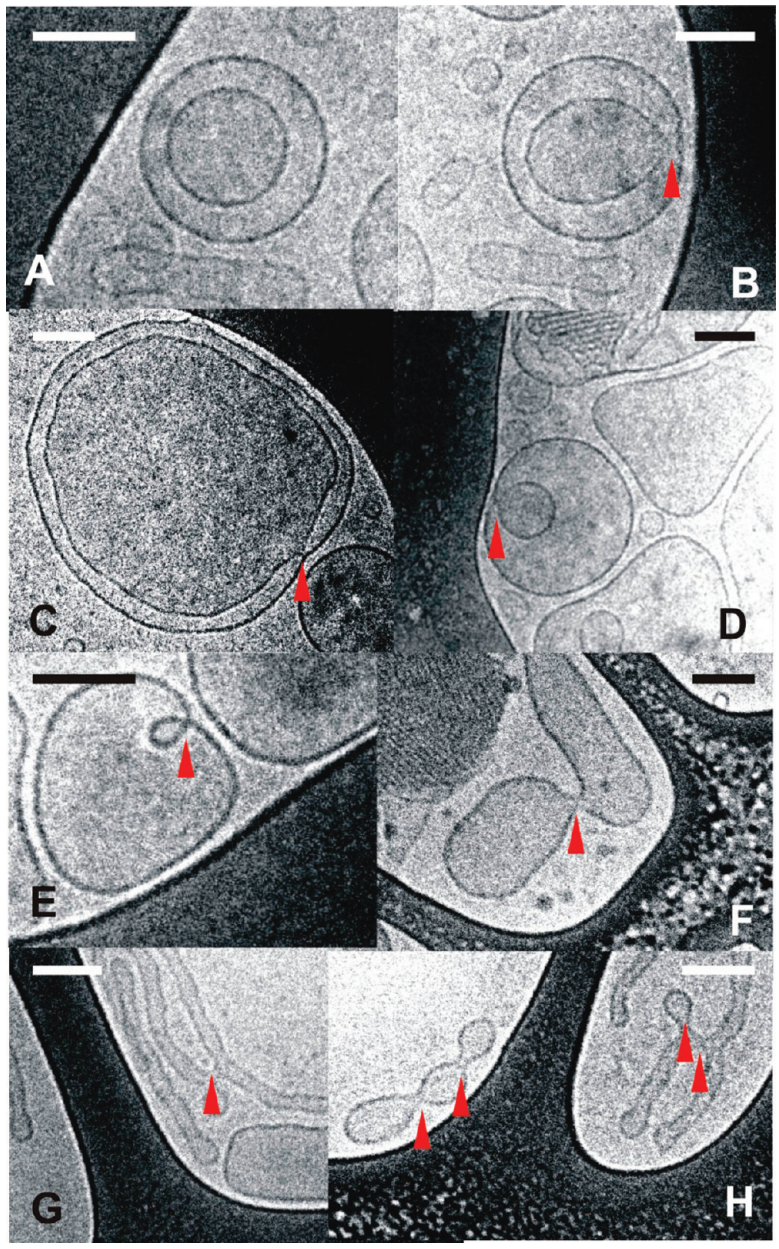

Figure 3. Cryo-TEM images of the sequence of events leading to membrane fusion. Important events are highlighted by the red arrowheads. Lipid 1 makes up 2 wt % of sample: (A) multilamellar vesicle; (B) thermal membrane undulations that allow the formation of membrane contacts as seen in panel C. Stalks are exemplified in panels D and E. (F−H) The formation of pores or interlamellar attachments, which also display a range in size and morphologies. (100 nm scale bars.)

phase.[19,24] Conn *et al*. in a SAXS study reported that a decrease in L_α spacing due to the formation of the membrane attachments was followed by a broad peak at low scattering angle, assigned to phase X.[19]

Both the lifetime and initial observable lattice parameter of phase X increase as the concentration of Poloxamer increases. We postulate that this is due to enhanced steric entropic interaction. Such a swollen intermediate coexisting with the L_α, has also been attributed to pore defects within the lamellar phase, which has sometimes been referred to as the random mesh phase.[25] As summarized in Supporting Information, Table S1, and visible in Figure 2, increasing the amount of Poloxamer increases the initial Q_{II}^D lattice parameter as the decreased transition rate allows an earlier observation of this phase. In conjunction higher block copolymer levels also induce a decrease in the equilibrium lattice parameter of the cubic Q_{II}^D phase. In contrast the presence of Poloxamer has little effect on the lattice parameter of the initial L_α phase.

Cryo-TEM, as described in the methods section of this article, was employed as a complementary technique to visualize the long-range-order of the metastable intermediates observed by SAXS and to observe disordered transformation structures. A cryo-TEM study of a 2 wt % nanoparticulate dispersion of lipid **1** in the presence of 0.2 wt % Poloxamer 407 and 5 wt % ethanol was performed, where wt % refers to weight percentages with respect to total sample mass. Ethanol is commonly used in dispersion preparation to facilitate the break up of the bulk amphiphilic aggregate.

Nanoparticulate dispersions of lipid **1** for cryo-TEM experiments were prepared at room temperature and then incubated at 37 °C which allowed us to capture the individual stages of conversion from the L_α to the Q_{II}^D phase. The first stage of the phase transformation process is the membrane fusion process to form an interlamellar attachment *via* a stalk intermediate.

Visualization of Membrane Fusion. ***Stalk Formation.*** The transition between the lamellar and cubic phase requires a distinct change in membrane topology. Figure 3 illustrates the process of creation of interlamellar attachments, with the arrowheads depicting key events in the sequence. Figure 3A shows a multilamellar vesicle, typical of those present in a fluid lamellar phase. Thermally induced membrane undulations are observable in Figure 3B and facilitate the rapprochement of two parallel membranes.[26] Figure 3C demonstrates a contact between two opposed membranes, showing notably the pointedness of the contact. The area of contact involved in this contact is sharper than the resolution of the microscope, typically approximately 2 nm. The thickness, or height of this contact increases as a stalk is formed, as shown in Figure 3D.

It is interesting to note that this series of events is a continuous process. There are constant changes in the curvature of the system and not a step by step quantized series of events. Yang and Huang reported the observation of an "equilibrium" stalk phase, with a morphology similar to the one shown here.[27] However we

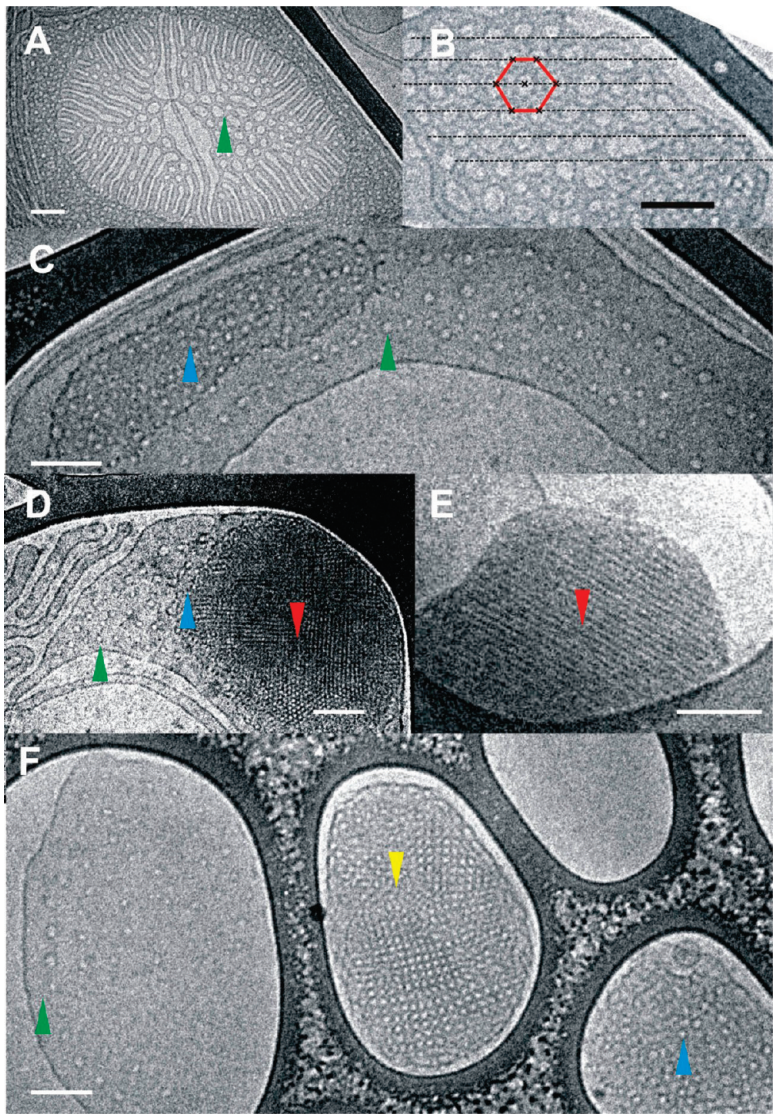

Figure 4. Cryo-TEM images displaying the "frame by frame" formation of Q_{II}^{D} *via* phase X; lipid 1 makes up 2 wt % of total sample mass. Formation of multiple interlamellar stalks (A) with green arrowheads showing the arrangement of pores. The vesicles have been transformed into a toroid of genus *n*, where *n* = number of pores or ILAs. The blue arrowheads highlight regions of 3D packed pores. The yellow arrowhead represents the swollen cubic intermediate-phase X. The red arrowhead in panels D and E displays the cubic phase lattice. (B) The increasing ordering of ILA alignment into a hexagonally packed square lattice. The lattice parameter of the pore and interpore spacing highlighted is 40 ± 2.6 nm. The progression from lamellar to cubic phase *via* ILA packing and swollen cubic phase intermediate is evident in panels C− E. (C,D, and F) The tight packing of these vesicles into a cubic-like lattice with an increased number of pores and water channels. Cubic phase with a final lattice parameter as obtained with synchrotron SAXS is highlighted by the red arrowheads in panels D and E. (F) Colloidal particles at different stages of phase transformation, from left to right: ILA packing, swollen cubic intermediate, and 3D ILA packing (100 nm scale bars).

are able to show a large variation in stalk and ILA size as the different structures mature.

Interlamellar Attachment Formation. Once the stalk contacts are established it is possible to follow their progression into interlamellar attachments, Figure 3E−H. These images distinctly resemble the model shown in Figure 1. Because of the observation of pores in other membranes of the same sample, Figure 3 panels D and E are assumed to demonstrate membrane contacts, and thus the vesicles are on the brink of increasing their genus to 1 rather than a folded vesicle which would retain genus 0.

Progression of the system's geometry to that of a cubic phase lattice requires ILA ordering. We propose that after the formation of one pore (or ILA), further attachments occur in a disorganized fashion, with limited or no long-range order. As more pores are formed these start to pack in a lowest energy configuration while maintaining preferential curvature—in either a cubic lattice or hexagonal lattice.[28] One can envisage the periodic stacking of such lattices to form close-packed hexagonal or close-packed cubic lattices, which can then go on to form a precursor to the intermediate mesophase: phase X shown in the SAXS data.

Visualization of Phase X. ***Formation of Multiple ILAs.*** Figure 4A shows that as the number of ILAs increase, the original vesicles become extremely distorted and start forming elongated structures. These structures bear very strong resemblance to cellular organelles such as the smooth endoplasmic reticulum and Golgi apparatus.[29−31] The alteration of the original shape may be attributed to volume loss due to leakage to take into account stress changes within the membrane (Figure 4A). This leads to the formation of a disorganized array of ILAs as shown in Figure 4A.

ILA Packing. Figure 4B shows configuration of the ILAs into a systematically packed structure, specifically identified by the green arrowheads in Figures 4C, 4D, and 4F. We note the variation in pore size and interpore distance observed for different aggregates, reflecting the different stages of transition. A typical hexagonally packed lattice is shown in Figure 4B. The interpore distance shown in this lattice is approximately 40 ± 2.6 nm (see Supporting Information, Figure S2).

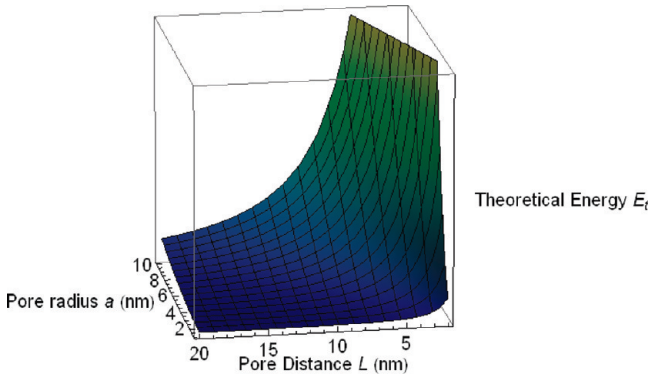

Figure 5. $E_t = 4\pi^2(a/L)^2$ where E_t is a simplified predicted theoretical energy of porous membranes, a is pore radius, and L is interpore distance. The plot clearly illustrates a model close to that of the repulsion of hard spheres as developed by Michalet *et al*. to assess the effect of pore size and interpore distance on the system.[28] It clearly illustrates that to allow close packing of the membrane pores suitable for the formation of an inverse bicontinuous cubic phase a significant reduction in ILA size is required.

Experimental studies on the structural dynamics of the fluid lamellar to the inverse bicontinuous cubic phase transition have been limited but significant relevant modeling experiments have been performed. Michalet *et al*. have provided a thorough discussion on the energetics of porous membranes, such as those presented here.[28] They conclude that pore to pore distance can be approximated to a length l_c, $l_c \approx (aL)^{1/2}$ where L is unit cell length and a is pore radius. Such a regular array of pores has a lower free energy than a random arrangement.[32] Initially we surmise that the ILAs are too large to accommodate the increased curvature stress present in the membrane, but that as suggested by Conn *et al*. the small curvature elastic energy associated with expanding channel size leads to an efficient method of increasing water flux through the sample.[19] Once the system is sufficiently hydrated, it is possible for the system to adopt the ideal curvature configuration, that is, a reduction in pore size and decreased interpore distance required for the system to adapt to the lipid's propensity to form a curved system. Michalet's theoretical energy (E_t) model $E_t = 4\pi^2(a/L)^2$, as plotted in Figure 5, supports our experimental observations that the vesicle size reduces (Figure 6B,C).

In agreement with these literature results, we have observed an ordered 2D hexagonally packed nanochannel network which can then pack in the third dimension to form a bicontinuous intermediate structure. The transformation to the initially packed state also resembles the hexagonally perforated morphology observed in lamellar to gyroid transitions observed in block copolymer assemblies.[33,34] The formation of stacked organized porous membrane is the next logical step in the formation of the cubic phase.

Smaller irregular pores (Figure 6A), with crescent moon-like shapes, represent ILAs that have just formed, while larger and often more circular pores represent mature pores. Simulation studies have suggested the existence of anisotropic stalk deformation inducing holes in the hemifusion diaphragm.[35,36] The irregular shapes may be indicative of their formation pathway, which from this evidence would seem to resemble more closely that of the transmembrane contact followed by hemifusion diaphragm rupture.[22]

Formation of Phase X. The stacked hexagonally packed lattice of ILAs shown in Figure 4 by the blue arrowheads develops into a convoluted structure which is difficult to resolve by TEM but has a smaller lattice parameter (Figure 6). It follows therefore that the structure observed in Figure 4B is the precursor to phase X, stacked layers of packed vesicles, essentially a complex foam-like network. The yellow arrowhead in Figure 4 highlights a self-assembled lipid nanoparticle with phase X morphology.

Different membrane perforation structure intermediates, phase X, and cubic phase are all shown in Figure 6 with their respective Fast Fourier transforms. Different levels of packing and size of repeat unit are distinctly observed. These results confirm the presence of the intermediate seen with SAXS, and matching of the lattice parameter (*e.g.*, 11 nm for the Q_{II}^D and 26−20

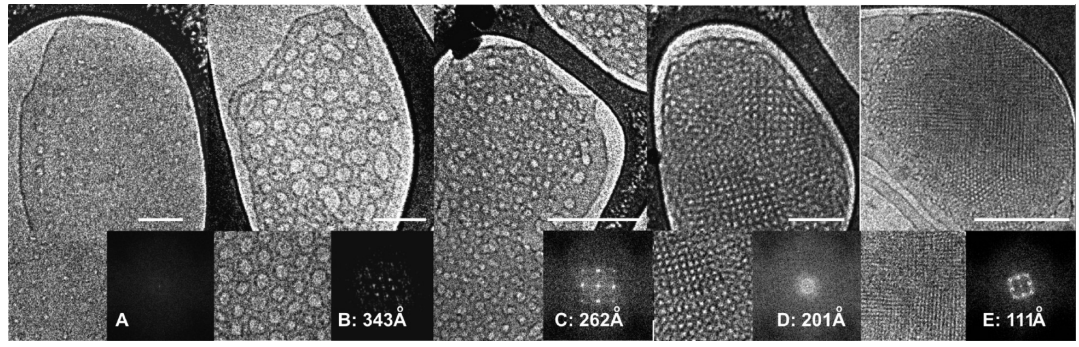

Figure 6. Cryo-TEM images of the progression of ILA organization into bicontinuous cubic phase from left to right. Fast Fourier transform show the changes in repeat unit: (A) no significant ordering; (B) hexagonally packed ILA lattice with large repeat unit; (C) two hexagonally packed lattices overlapping to form a cubic phase precursor (phase X). The repeat unit of this is similar to that observed by SAXS (see Figure 2). (D) An example of the swollen cubic lattice also observed with SAXS; (E) final Q_{II}^D lattice with a lattice parameter corroborating that measured with synchrotron small-angle X-ray scattering. (100 nm scale bars.)

nm for phase X) allows direct correlation between the two independently acquired data sets. The SAXS and cryo-TEM are, in this instance, complementary techniques. These observations also corroborate the SAXS derived lattice parameter of phase X previously reported of around 20 nm.[19]

Phase X can in turn alter its topology in order to adopt the swollen cubic phase, in this case the Q_{II}^{D} phase, which will support the desired curvature prior to reaching equilibrium curvature values.

Formation of Q_{II}^{D} Phase. The red arrowheads in Figure 4 highlight the presence of large domains of Q_{II}^{D} phase. These domains match precisely the geometry of the 100 Bravais lattice plane as described by Almsherqi *et al.*[14] Figure 6E demonstrates that the observed final cubic phase has a similar lattice parameter to that measured with synchrotron SAXS.

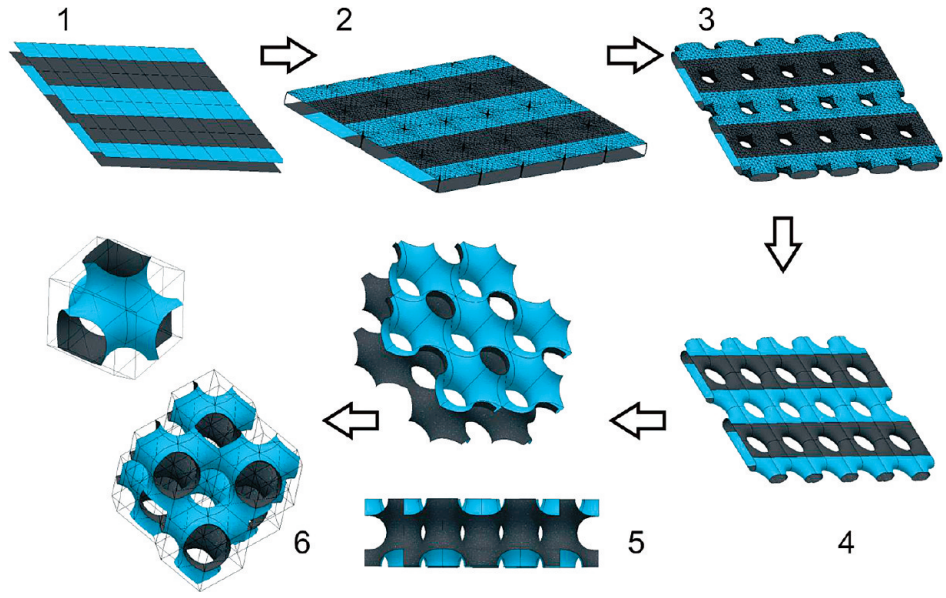

Figure 7. Schematic representation of the major transformation stages involved in the creation of a bicontinuous cubic structure from a planar lamellar structure. These surfaces were plotted using Surface Evolver.[38] (1) Lamellar phase: each plane represents a lipid bilayer. The membrane bilayer undergoes thermal undulations which allow the formation of membrane contacts. These membrane contacts can develop into stalks (2). These proceed to form ILAs (pores) (3). To form the cubic phase these pores order into a hexagonally packed lattice (4) which can pack in 3D to form phase X as observed in our SAXS kinetic studies (5). Phase X consists of layers of hexagonally packed pores forming a 3D lattice with two distinct water channels. This can then further pack into a cubic lattice, initially with high water content ("swollen") which will then reach an equilibrium lattice size and curvature characteristic of a Q_{II}^{D} (*Pn3m*) cubic phase (6).

According to our experimental observations it is possible to propose the following model for cubic phase formation from a lamellar phase (Figure 7): (1) membrane undulations and (2) formation of stalks; (3) interlamellar attachments (ILAs) *via* hemifusion rupture; (4) ILA alignment and reduction in size - precursor to phase X; (5) phase X formation; (6) formation of cubic lattice *via* swollen intermediate.

Figure 7 cannot illustrate the dynamic and flowing aspects of the membrane fusion process, outlined by Weinreb *et al*., and the cubic phase formation.[37] Figure 7 does, however, illustrate the types of intermediate self-assembly structures that we have observed and serves to link them into a coherent sequence of transformation events.

Our experiments in part show complementary results to those of Yang *et al*. but, whereas their results relate to an equilibrium phase of stalks, we have here directly shown the nonordered, early formation of stalks during a dynamic process.[27]

The presence of the block copolymer, Poloxamer 407, acts as a stabilizer of the intermediates observed by sterically hindering rapid packing of the ILAs and potentially by relieving curvature stresses present in the membrane. The nucleation and growth of the long-range ordered intermediate appears to be slower when the Poloxamer and lipid derivative **1** are codispersed.

Visualization of the elusive intermediate phase was only possible here due to the use of dispersed nanoparticulate vesicles (liposomes). Bulk phase samples would preclude the observation of these pore arrays due to the thickness of the sample and focusing difficulties.

Siegel has previously reported that as the various inverse bicontinuous cubic phases are almost isoenergetic; thus one can postulate that other inverse bicontinuous cubics occur *via* similar intermediates.[39] The intermediate structures are able to modulate the curvature stress and allow the development of 3D interfaces. The intermediate of packed ILAs allows the formation of the cubic phase and may also be one of the intermediates present during the transition from the L_{α} to the inverse hexagonal (H_{II}) phase. It has been suggested that trans-monolayer contacts (hemifusion contacts) aggregate into a body centered or primitive tetragonal lattice.[22,40] Our data clearly shows that there are a range of precursors that are formed with varying packing density and curvatures. The structural parameters of the aligned ILA structure will vary according to the free energy of the system and this will be directly dependent on the spontaneous curvature and bending rigidity of the lipid self-assembly object.

CONCLUSION

In a cell biology context, the experimental confirmation of the intermediate lipid self-assembly structures advances the understanding of organelle morphogene-

sis and maturation as well as dynamic processes such as endo/exocytosis. Cells may use similar steric effects, using membrane proteins for example, to control shape changes in membranes and mechanically affect rates of membrane reconfiguration.

The manipulation of intermediate structures in nanoparticulate dispersions of lipid self-assembly phases may provide a unique system for encapsulation and controlled release of bioactives. The ability to control intermediate transformations may also allow the development of flexible growth media for applications such as in-cubo integral membrane protein crystallization or liquid crystal templating of nanostructured materials. Advancing the understanding of how amphiphiles order and build complex structures, using low-energy transformation processes, will undoubtedly assist in designing improved bottom-up nanofabrication processes to create novel high-performance functional amphiphile self-assembly materials.

METHODS

Materials. The synthesized nucleolipid, 5′-deoxy-5-fluoro-N^4-(cis-9-octadecenyloxy-carbonyl) cytidine, (Figure 1) was used as the lipid in the system. The water used in the hydration of the samples was double distilled water with 18.2 MΩ resistance. The triblock copolymer Poloxamer 407 (see Supporting Information, Figure S1) was obtained from Sigma (St Louis, MO) and used without further purification.

Preparation of Lipid 1 Nanoparticulate Dispersions for cryo-TEM. To form the nanoparticulate dispersions for cryo-TEM imaging, lipid **1** and 10 wt % (based on lipid mass) of triblock copolymer were initially dissolved in the minimum amount of absolute ethanol. The ethanol aids in lipid dispersion. This mixture was added dropwise to water with vigorous shaking to achieve a final composition: 2.3 wt % lipid **1**, 0.2 wt % Poloxamer 407, 4.9 wt % ethanol, and 92.6 wt % water. Following sonication in a benchtop sonicator the colloidal dispersion was then extruded with a 100 nm polycarbonate filter (Mini-extruder, Avanti Polar lipids). The sample was found to be homogeneous by dynamic light scattering sizing after 30 cycles (data not shown). The amphiphile particles will remain stable and dispersed (with a ratio of at least 9:1 amphiphile/stabilizer) for several days before aggregation is observed.

Cryo-TEM Experiments. To observe the lamellar (liposome) to cubic (cubosome) phase transition, vitrification was performed at 37 °C with 90% humidity atmosphere in a custom-built environmental chamber. Samples were prepared for imaging by cryo-TEM according to the method of Adrian *et al.*[41] A 4−5 μL portion of sample solution was applied to a 300 mesh copper TEM grid coated with a lacey carbon film (ProSciTech, Thuringowa Qld 4817, Australia) and allowed to settle for 30 s. The grid was manually blotted for 10−15 s, and the resulting thin film was then vitrified by plunging into liquid ethane. Grids were stored in liquid nitrogen before transferring into a Gatan 626-DH Cryo-holder. Imaging was carried out using an FEI Tecnai 12 TEM, operating at 120 kV, equipped with a MegaView III CCD camera and AnalySis imaging software (Olympus Soft Imaging Solutions). The sample was kept at a temperature of −180 °C and standard low-dose procedures were used to minimize radiation damage.

Preparation of Lipid 1 Nanoparticulate Dispersions for Synchrotron Small Angle X-ray Scattering (SAXS). To form the nanoparticulate dispersions for SAXS, lipid **1**, 10 wt % of total sample mass and varying levels (0, 0.5, 1 wt % of total sample mass and 1 wt % Poloxamer 407 + ethanol (5 wt % of total sample mass)) of the Poloxamer 407 were initially dissolved in water. Lipid **1** was added to the Poloxamer solution and sonicated in a bath sonicator for 5 min. A sonicator probe was then used with 5 s pulses and 20 s rest period for a total time of 5 min. The final nanoparticulate dispersion was a milky suspension with no aggregates. Final lipid **1** concentration was 10 wt %.

Synchrotron SAXS. The Australian synchrotron SAXS beamline was used to perform SAXS experiments. The synchrotron X-ray beam was tuned to a wavelength of 0.8266 Å with a typical flux of 1013 photon/sec. The 2-D diffraction patterns were recorded on a Bruker 6000 CCD detector. The detector was offset to access a greater q-range. Silver behenate (a = 58.38 Å) was used as the low-angle X-ray diffraction calibrant for all measurements.

Diffraction images were analyzed by the IDL-based AXcess software package, developed at Imperial College, London, by Dr. A. Heron.[20] The measured X-ray spacings are accurate to within 0.1 Å. The temperature control was achieved in a custom designed peltier driven cell with temperature control of ±0.1 °C. Samples were loaded in 1.5 mm special glass capillaries.

Acknowledgment. C.J.D. is the recipient of an Australian Research Council Federation Fellowship. X.J.G. is the recipient of a CSIRO Ph.D. studentship. C.J.D. thanks J. Seddon for discussions regarding the Cryo-TEM results while C.J.D. was a visiting scientist at Imperial College, London, in July 2008. This visit was supported by an Australian Academy of Science travel grant. Part of this research was undertaken on the SAXS beamline at the Australian Synchrotron, Victoria, Australia. The views expressed herein are those of the authors and are not necessarily those of the owner or operator of the Australian Synchrotron. We thank beamline scientists, Nigel Kirby and Stephen Mudie, for assistance during data collection.

Supporting Information Available: Figures S1 and S2. This material is available free of charge *via* the Internet at http://pubs.acs.org.

REFERENCES AND NOTES

1. Luzzati, V.; Tardieu, A.; Gulikkrz, T. Polymorphism of Lipids. *Nature* **1968**, *217*, 1028–1030.
2. Mulet, X.; Templer, R. H.; Woscholski, R.; Ces, O. Evidence that Phosphatidylinositol Promotes Curved Membrane Interfaces. *Langmuir* **2008**, *24*, 8443–8447.
3. Clogston, J.; Caffrey, M. Controlling Release From the Lipidic Cubic Phase. Amino Acids, Peptides, Proteins, and Nucleic Acids. *J. Controlled Release* **2005**, *107*, 97–111.
4. Angelova, A.; Ollivon, M.; Campitelli, A.; Bourgaux, C. Lipid Cubic Phases as Stable Nanochannel Network Structures for Protein Biochip Development: X-ray Diffraction Study. *Langmuir* **2003**, *19*, 6928–6935.
5. Yang, D.; Armitage, B.; Marder, S. R. Cubic Liquid-Crystalline Nanoparticles. *Angew. Chem., Int. Ed.* **2004**, *43*, 4402–4409.
6. Conn, C. E.; Ces, O.; Squires, A. M.; Mulet, X.; Winter, R.; Finet, S. M.; Templer, R. H.; Seddon, J. M. A Pressure-Jump Time-Resolved X-ray Diffraction Study of Cubic−Cubic Transition Kinetics in Monoolein. *Langmuir* **2008**, *24*, 2331–2340.
7. Drummond, C. J.; Fong, C. Surfactant Self-Assembly Objects as Novel Drug Delivery Vehicles. *Curr. Opin. Colloid Interface Sci.* **1999**, *4*, 449–456.
8. Larsson, K. Cubic Lipid−Water Phases—Structures and Biomembrane Aspects. *J. Phys. Chem.* **1989**, *93*, 7304–7314.
9. Shearman, G. C.; Ces, O.; Templer, R. H.; Seddon, J. M. Inverse Lyotropic Phases of Lipids and Membrane Curvature. *J. Phys.: Condens. Matter* **2006**, *18*, S1105–S1124.
10. Braun, P. V.; Stupp, S. I. CdS Mineralization of Hexagonal, Lamellar, and Cubic Lyotropic Liquid Crystals. *Mater. Res. Bull.* **1999**, *34*, 463–469.

11. Nollert, P.; Qiu, H.; Caffrey, M.; Rosenbusch, J. P.; Landau, E. M. Molecular Mechanism for the Crystallization of Bacteriorhodopsin in Lipidic Cubic Phases. *FEBS Lett.* **2001**, *504*, 179–186.
12. Cherezov, V.; Rosenbaum, D. M.; Hanson, M. A.; Rasmussen, S. G.; Thian, F. S.; Kobilka, T. S.; Choi, H. J.; Kuhn, P.; Weis, W. I.; Kobilka, B. K.; Stevens, R. C. High-Resolution Crystal Structure of an Engineered Human β2-Adrenergic G Protein-Coupled Receptor. *Science* **2007**, *318*, 1258–1265.
13. Almsherqi, Z. A.; Landh, T.; Kohlwein, S. D.; Deng, Y. Chapter 6: Cubic Membranes—The Missing Dimension of Cell Membrane Organization. *Int. Rev. Cell Mol. Biol.* **2009**, *274*, 275–342.
14. Almsherqi, Z. A.; Kohlwein, S. D.; Deng, Y. Cubic Membranes: A Legend Beyond the Flatland of Cell Membrane Organization. *J. Cell. Biol.* **2006**, *173*, 839–844.
15. Landh, T. From Entangled Membranes to Eclectic Morphologies: Cubic Membranes as Subcellular Space Organizers. *FEBS Lett.* **1995**, *369*, 13–17.
16. McMahon, H. T.; Gallop, J. L. Membrane Curvature and Mechanisms of Dynamic Cell Membrane Remodelling. *Nature* **2005**, *438*, 590–596.
17. Norlen, L. Skin Barrier Formation: The Membrane Folding Model. *J. Invest. Dermatol.* **2001**, *117*, 823–829.
18. Norlen, L.; Al-Amoudi, A.; Dubochet, J. A Cryotransmission Electron Microscopy Study of Skin Barrier Formation. *J. Invest. Dermatol.* **2003**, *120*, 555–560.
19. Conn, C. E.; Ces, O.; Mulet, X.; Finet, S.; Winter, R.; Seddon, J. M.; Templer, R. H. Dynamics of Structural Transformations between Lamellar and Inverse Bicontinuous Cubic Lyotropic Phases. *Phys. Rev. Lett.* **2006**, *96*, 108102.
20. Seddon, J. M.; Squires, A. M.; Conn, C. E.; Ces, O.; Heron, A. J.; Mulet, X.; Shearman, G. C.; Templer, R. H. Pressure-Jump X-ray Studies of Liquid Crystal Transitions in Lipids. *Phil. Trans. R. Soc., A* **2006**, *364*, 2635–2655.
21. Leikin, S. L.; Kozlov, M. M.; Chernomordik, L. V.; Markin, V. S.; Chizmadzhev, Y. A. Membrane-Fusion—Overcoming of the Hydration Barrier and Local Restructuring. *J. Theor. Biol.* **1987**, *129*, 411–425.
22. Siegel, D. P. The Modified Stalk Mechanism of Lamellar/Inverted Phase Transitions and Its Implications for Membrane Fusion. *Biophys. J.* **1999**, *76*, 291–313.
23. Johnsson, M.; Edwards, K. Phase Behavior and Aggregate Structure in Mixtures of Dioleoylphosphatidylethanolamine and Poly(ethylene glycol)-Lipids. *Biophys. J.* **2001**, *80*, 313–323.
24. Caffrey, M. Kinetics and Mechanism of the Lamellar Gel/Lamellar Liquid-Crystal and Lamellar/Inverted Hexagonal Phase Transition in Phosphatidylethanolamine: A Real-Time X-ray Diffraction Study Using Synchrotron Radiation. *Biochemistry* **1985**, *24*, 4826–4844.
25. Oradd, G.; Gustafsson, J.; Almgren, M. Intermediate Phases in the System Egg Lecithin/CTAC/Brine. SAXS and NMR Studies. *Langmuir* **2001**, *17*, 3227–3234.
26. Helfrich, W. Effect of Thermal Undulations on the Rigidity of Fluid Membranes and Interfaces. *J. Phys. (Paris)* **1985**, *46*, 1263–1268.
27. Yang, L.; Huang, H. W. Observation of a Membrane Fusion Intermediate Structure. *Science* **2002**, *297*, 1877–1879.
28. Michalet, X.; Bensimon, D.; Fourcade, B. Fluctuating Vesicles of Nonspherical Topology. *Phys. Rev. Lett.* **1994**, *72*, 168–171.
29. Donohoe, B. S.; Mogelsvang, S.; Staehelin, L. A. Electron Tomography of ER, Golgi and Related Membrane Systems. *Methods* **2006**, *39*, 154–162.
30. Staehelin, L. A.; Kang, B. H. Nanoscale Architecture of Endoplasmic Reticulum Export Sites and of Golgi Membranes as Determined by Electron Tomography. *Plant Physiol.* **2008**, *147*, 1454–1468.
31. Morre, D. J.; Mollenhauer, H. H. Microscopic Morphology and the Origins of the Membrane Maturation Model of Golgi Apparatus Function. *Int. Rev. Cytol.* **2007**, *262*, 191–218.
32. Charitat, T.; Fourcade, B. Lattice of Passages Connecting Membranes. *J. Phys. II* **1997**, *7*, 15–35.
33. Hajduk, D. A.; Gruner, S. M.; Rangarajan, P.; Register, R. A.; Fetters, L. J.; Honeker, C.; Albalak, R. J.; Thomas, E. L. Observation of a Reversible Thermotropic Order−Order Transition in a Diblock Copolymer. *Macromolecules* **1994**, *27*, 490–501.
34. Hajduk, D. A.; Takenouchi, H.; Hillmyer, M. A.; Bates, F. S.; Vigild, M. E.; Almdal, K. Stability of the Perforated Layer (PL) Phase in Diblock Copolymer Melts. *Macromolecules* **1997**, *30*, 3788–3795.
35. Ellens, H.; Bentz, J.; Szoka, F. C. Destabilization of Phosphatidylethanolamine Liposomes at the Hexagonal Phase Transition Temperature. *Biochemistry* **1986**, *25*, 285–294.
36. Noguchi, H.; Takasu, M. Self-Assembly of Amphiphiles into Vesicles: A Brownian Dynamics Simulation. *Phys. Rev. E* **2001**, *64*, 041913.
37. Weinreb, G.; Lentz, B. R. Analysis of Membrane Fusion as a Two-State Sequential Process: Evaluation of the Stalk Model. *Biophys. J.* **2007**, *92*, 012–4029.
38. Brakke, K. A. *The Surface Evolver.* **1992**, *1*, 141–165.
39. Siegel, D. P. Inverted Micellar Intermediates and the Transitions Between Lamellar, Cubic, and Inverted Hexagonal Amphiphile Phases. III. Isotropic and Inverted Cubic State Formation *via* Intermediates in Transitions Between L Alpha and HII Phases. *Chem. Phys. Lipids* **1986**, *42*, 279–301.
40. Siegel, D. P.; Epand, R. M. The Mechanism of Lamellar-to-Inverted Hexagonal Phase Transitions in Phosphatidylethanolamine: Implications for Membrane Fusion Mechanisms. *Biophys. J.* **1997**, *73*, 3089–3111.
41. Adrian, M.; Dubochet, J.; Lepault, J.; Mcdowall, A. W. Cryo-electron Microscopy of Viruses. *Nature* **1984**, *308*, 32–36.